A REDUCED-RANK SQUARE ROOT FILTERING FRAMEWORK FOR NONINVASIVE FUNCTIONAL IMAGING OF VOLUMETRIC CARDIAC ELECTRICAL ACTIVITY

Linwei Wang[1]*, Heye Zhang*[2]*, Ken C.L. Wong*[1]*, and Pengcheng Shi*[1]

[1] Computational Biomedicine Lab, Rochester Institute of Technology, Rochester, NY, USA
[2] Bioengineering Institute, University of Auckland, Auckland

ABSTRACT

To noninvasively reconstruct transmembrane potential (TMP) dynamics throughout the 3D myocardium using body surface potential recordings, it is necessary to combine prior physiological models and patient's data with regard to their respective uncertainties. To fulfill model-data melding for this large-scale and high-dimensional system, data assimilation with proper computational reduction is needed for computational feasibility and efficiency. In this paper, we develop a reduced-rank square root TMP estimation algorithm, using dominant components of estimation uncertainties to guide a more efficient model-data coupling in the square root structure. The SVD-based reduced-rank error covariance is used to represent and track the dominant estimation errors, and unified into an integrated square root filtering framework. Phantom experiments demonstrate the ability of this framework to bring substantial computational reduction at slight expense of degraded estimation accuracy. It therefore improves the efficiency and applicability of the volumetric myocardial TMP imaging in practice.

Index Terms— Computational reduction, inverse problem of electrocardiography, body surface potential

1. INTRODUCTION

It has been desirable but challenging to noninvasively reconstruct transmembrane potential (TMP) dynamics throughout the 3D myocardium from body surface potential (BSP) recordings, which requires the coupling of general physiological models and patient's data with regard to their respective uncertainties. We adopt the unscented Kalman filter (UKF) [1] to develop the TMP estimation algorithm based on the combination of Monte Carlo (MC) methods and KF update rules [2]. It preserves the high-nonlinearity of the system dynamics and ensure the computational feasibility. However, regarding the large-scale and high-dimension of this problem, further improvement on the algorithm efficiency is desired.

Efforts in computational reduction of data assimilation for large-scale system have been long-lasting. In general, it is achieved either by a simplification of system dynamics [3], or the approximation of error covariance by, for instance, representing it on a coarser grid [4] or reducing its rank by truncation[5]. In comparison, approximation of error covariances is a favorable option for the TMP imaging problem because of the high nonlinearity of TMP dynamics and the less knowledge about model and data uncertainties.

Meanwhile, a square root (SR) structure is desirable for preventing filtering divergence and improving its numerical stability. Furthermore, it avoids the square root computation when generating ensemble from the SR of error covariances. Most existent SR filters are based on the cholesky factorization of error covariance matrices [6], leading to an upper triangular matrix which does not allow simple approximation. As a result, though more robust, these filters in general are not more efficient than their standard counterparts.

In this paper, we develop an integrated reduced-rank square root (RRSR) TMP estimation algorithm where this large-scale model-data melding is guided by the dominant components of full estimation uncertainties. The RR error model is introduced into the UKF and unified with the SR filtering structure. Phantom experiments are performed to evaluate the accuracy and computational efficiency of this RRSR TMP estimation algorithm, demonstrating its ability to bring substantial reduction of computational times with slight degrading of estimation accuracy. It improves the efficiency and applicability of volumetric myocardial TMP imaging.

2. PHYSIOLOGICAL-MODEL-CONSTRAINED BAYESIAN PARADIGM FOR 3D TMP IMAGING

2.1. Cardiac electrophysiological system

A coupled meshfree-BEM platform is developed to represent personalized combined heart-torso structure, where the 3D myocardium is described by a cloud of meshfree points and the torso by triangulated body surface [7]. This system consists of a dynamic model for general physiological knowledge on volumetric TMP activity (TMP activity model (1)), and an observation model relating latent volumetric TMPs to external BSP observations (TMP-to-BSP model (2)) [7].

$$\begin{cases} \frac{\partial \mathbf{U}}{\partial t} = -\mathbf{M}^{-1}\mathbf{K}\mathbf{U} + f_1(\mathbf{U},\mathbf{V}) \\ \frac{\partial \mathbf{V}}{\partial t} = f_2(\mathbf{U},\mathbf{V}) \end{cases} \tag{1}$$

$$\mathbf{\Phi} = \mathbf{H}\mathbf{U} \tag{2}$$

where $\mathbf{U}$ and $\mathbf{V}$ are vectors composed of TMP and recovery current from all meshfree points, and Φ contains BSP on all boundary element vertices on the body surface. Matrices $\mathbf{M}$ and $\mathbf{K}$ are constructed based on the meshfree method, accounting for the intercellular coupling of electrical propagation. They encode 3D myocardial structure and its conductive anisotropy. $f_1(\mathbf{U},\mathbf{V})$ and $f_2(\mathbf{U},\mathbf{V})$ describe TMP shapes on each meshfree point and include electrical heterogeneity across the heart wall. The transfer matrix $\mathbf{H}$ is developed based on the coupling of BEM and meshfree strategy, encoding all the anatomical and conductivity information in personalized heart and torso structures.

2.2. Stochastic state-space formulation

There are always discrepancies between general physiological models and patient-specific conditions, and data errors always arise in the practice of body surface mapping. To explicitly allow these uncertainties to exist, the physiological system is reformulated into a state space representation. With the state vector $\mathbf{X}(t) = \left(\mathbf{U}(t)^T\mathbf{V}(t)^T\right)^T$ and the measurement vector $\mathbf{Y}(t) = \mathbf{\Phi}(t)$, additive stochastic components $\omega(t)$ and $\nu(t)$ are introduced into (1) and (2) respectively:

$$\frac{\partial \mathbf{X}(t)}{\partial t} = \begin{pmatrix} -\mathbf{M}^{-1}\mathbf{K} & \mathbf{0} \\ \mathbf{0} & \mathbf{0} \end{pmatrix} \mathbf{X}(t) + \begin{pmatrix} f_1(\mathbf{X}(t)) \\ f_2(\mathbf{X}(t)) \end{pmatrix} + \omega(t) \quad (3)$$

$$\mathbf{Y}(t) = \begin{pmatrix} \mathbf{H} & \mathbf{0} \end{pmatrix} \mathbf{X}(t) + \nu(t) = \tilde{\mathbf{H}}\mathbf{X}(t) + \nu(t) \quad (4)$$

Since BSP data are collected by discrete sampling, the continuous state space system (3,4) is discretized in time with k denoting the sampling index:

$$\mathbf{X}_k = F_d(\mathbf{X}_{k-1}) + \omega_k \quad (5)$$

$$\mathbf{Y}_k = \tilde{\mathbf{H}}\mathbf{X}_k + \nu_k \quad (6)$$

where a fourth-order Runge-Kutta solver is embedded in the filtering process for temporal discretization of (5).

2.3. Standard TMP estimation algorithm

The main concerns for developing an appropriate TMP estimation algorithm arise from 1), the strong nonlinearity of (3); 2), the implicit temporal discretization of (3) during the filtering; and 3), the high-dimension and large-scale of the system. We adopt the idea of the UKF [1] to develop a two-step prediction-correction filtering framework: regarding the aforementioned nature of the state model (5), the prediction of $\mathbf{X}_k$ is performed in a MC manner and the ensemble is selected in a deterministic way according to the unscented transform [1]. Based on the linear measurement model (6), the estimation of $\mathbf{X}_k$ given available data follows the KF update rules. The algorithm at the kth iteration is outline as follows:

1. Selection of weighted ensemble set $\{\mathcal{X}_{k,i}, W_i\}_{i=0}^{2n}$:
   $\{\mathcal{X}_{k,i}\}_{i=0}^{2n} = \left(\hat{\mathbf{X}}_k \quad \hat{\mathbf{X}}_k \pm \sqrt{(n+\lambda)\hat{\mathbf{P}}_{x_k}}\right)$

2. Prediction:
   $\mathcal{X}_{k+1|k,i} = \tilde{F}_d(\mathcal{X}_{k,i})$
   $\bar{\mathbf{X}}_{k+1}^- = \sum_{i=0}^{2n} W_i^m \mathcal{X}_{k+1|k,i}$
   $\mathbf{P}_{x_{k+1}}^- = \sum_{i=0}^{2n} W_i^c(\mathcal{X}_{k+1|k,i} - \bar{\mathbf{X}}_{k+1}^-)(\mathcal{X}_{k+1|k,i} - \bar{\mathbf{X}}_{k+1}^-)^T + \mathbf{Q}_{\omega_{k+1}}$

3. Correction:
   $\mathbf{G}_{k+1} = \mathbf{P}_{x_{k+1}}^- \tilde{\mathbf{H}}^T(\tilde{\mathbf{H}}\mathbf{P}_{x_{k+1}}^- \tilde{\mathbf{H}}^T + \mathbf{R}_{\nu_{k+1}})^{-1}$
   $\hat{\mathbf{X}}_{k+1} = \bar{\mathbf{X}}_{k+1}^- + \mathbf{G}_{k+1}(\mathbf{Y}_{k+1} - \tilde{\mathbf{H}}\bar{\mathbf{X}}_{k+1}^-)$
   $\hat{\mathbf{P}}_{x_{k+1}} = (\mathbf{I} - \mathbf{G}_{k+1}\tilde{\mathbf{H}})\mathbf{P}_{x_{k+1}}^-$

where $\bar{\mathbf{X}}_{k+1}^-$ and $\mathbf{P}_{x_{k+1}}^-$ are the predicted mean and covariance of $\mathbf{X}_{k+1}$, while $\hat{\mathbf{X}}_{k+1}$ and $\hat{\mathbf{P}}_{x_{k+1}}$ are the corresponding final estimates. $\mathbf{Q}_{\omega_{k+1}}$ and $\mathbf{R}_{\nu_{k+1}}$ are the predefined error covariances of ω_{k+1} and ν_{k+1} . n is the dimension of $\mathbf{X}$, and parameter λ is determined by n. As demonstrated in our previous works, this algorithm provides feasible noninvasive TMP imaging in practice [2]. Nevertheless, regarding the high-dimensionality and large-scale of this problem, improvement in computational efficiency and stability is desired.

3. REDUCED-RANK SQUARED-ROOT FILTERING

The fundamental of this computational reduction is utilizing dominant components of estimation uncertainties to guide the model-data melding in a SR structure.

3.1. Definitions

Reduced-rank error model: The evolution of error covariance $\mathbf{P}_x$ represents the interaction of models, data and their uncertainties during the estimation. Therefore, a careful reduction of it can account for the majority of the uncertainties and guide the model-data coupling in a more efficient manner. Besides, since the model and data uncertainties are usually not well-known, a proper reduction is sensible for the sake of computational efficiency.

Since the current algorithm is based on the minimum-mean-square-error criterion, the reduced-rank approximation of $\mathbf{P}_x$, $\mathbf{P}_x^q$, should minimize the 2-norm of the residual error covariance. The rank-q SVD of $\mathbf{P}_x$ is a suitable option for this purpose. Because $\mathbf{P}_x$ is symmetric, its SVD reduces to eigen-decomposition $\mathbf{P}_{x_k} = \mathbf{V}_k\mathbf{D}_k\mathbf{V}_k^T$, where the diagonal matrix $\mathbf{D}_k$ contains all the eigenvalues and $\mathbf{V}_k$ the corresponding eigenvectors. Let $\mathbf{D}_k^q$ consist of the first q leading eigenvalues and $\mathbf{V}_k^q$ the corresponding eigenvectors, the reduced-rank error model is defined as $\mathbf{P}_{x_k}^q = \mathbf{V}_k^q\mathbf{D}_k^q\mathbf{V}_k^{q\,T}$.

Square root structure: Instead of the widely-used Cholesky decomposition, we present an alternative SR of $\mathbf{P}_{x_k}$, $\mathbf{S}_{x_k}$, so that it could be unified with the SVD-based reduced-rank error model: The reduced-rank approximation of $\mathbf{S}_x$ is straightforward: $\mathbf{S}_{x_k}^q = \mathbf{V}_k^q\sqrt{\mathbf{D}_k^q}$. Based on these two definitions, the reduced-rank filtering and SR structure could be unified into an integrated formulation.

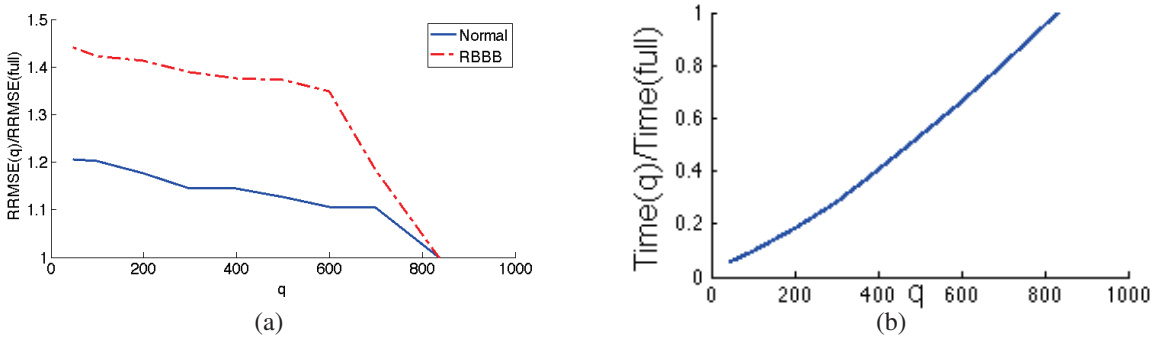

(a) (b)

Fig. 1. (a) TMP estimation accuracy (RRMSE) with increasing number of rank (q), divided by RRMSE in full-rank filtering. (b) Computational time with increasing number of rank (q), divided by computational time in full-rank filtering.

3.2. Reduced-rank square-root (RRSR) filtering

Ensemble selection: Under the guidance of reduced-rank SR of the error covariance ($\hat{\mathbf{S}}^q_{x_k}$), the ensemble at kth iteration is selected according to the distribution of principle error components:

$$\{\mathcal{X}_{k,i}\}_{i=0}^{2q} = \left(\hat{\mathbf{X}}_k \quad \hat{\mathbf{X}}_k \pm \sqrt{(q+\lambda^q)}\hat{\mathbf{S}}^q_{x_k}\right) \tag{7}$$

Because q normally $\ll n$, the ensemble size is substantially reduced. It brings substantial computational reduction, since the most expensive computation in the original algorithm comes from the propagation of individual ensemble member through the state model.

Prediction: This ensemble set propagates through the state model and predicts the mean and error covariance of $\mathbf{X}_{k+1}$. Based on the SR structure, $\mathbf{S}^-_{x_{k+1}}$ can be directly obtained without computing the full error covariance $\mathbf{P}^-_{x_{k+1}}$:

$$\begin{aligned}
\mathcal{X}_{k+1|k,i} &= \tilde{F}_d(\mathcal{X}_{k,i}) \qquad (8)\\
\bar{\mathbf{X}}^-_{k+1} &= \sum_{i=0}^{2q} W_i \mathcal{X}_{k+1|k,i}\\
\mathbf{S}^-_{x_{k+1}} &= \left(\sqrt{W_i}(\mathcal{X}_{k+1|k,i} - \bar{\mathbf{X}}^-_{k+1})_{i=0:2q} \quad \sqrt{\mathbf{Q}_{\omega_{k+1}}}\right)
\end{aligned}$$

To track the dominant components of the error covariance after the incorporation of additional model errors $\mathbf{Q}_{\omega_{k+1}}$, $\mathbf{S}^-_{x_{k+1}}$ is projected onto the subspace spanned by the q dominant eigenvectors of $\mathbf{P}^-_{x_{k+1}}$:

$$\mathbf{S}^{q-}_{x_{k+1}} = \mathbf{S}^-_{x_{k+1}}\mathbf{V}^q_{k+1} \tag{9}$$

where $\mathbf{V}^q_{k+1}$ can be directly calculated by q-rank SVD on $\mathbf{S}^-_{x_{k+1}}$ as $\mathbf{U}^q_{k+1}\mathbf{D}^q_{k+1}\mathbf{V}^{qT}_{k+1}$.

Correction: Rewriting the KF update equations in SR formulations:

$$\hat{\mathbf{S}}_{x_{k+1}}\hat{\mathbf{S}}^T_{x_{k+1}} = \mathbf{S}^-_{x_{k+1}}(\mathbf{I} - \tilde{\mathbf{K}}_{k+1}\tilde{\mathbf{C}}_{k+1})\mathbf{S}^{-T}_{x_{k+1}} \tag{10}$$

where $\tilde{\mathbf{K}}_{k+1} = \tilde{\mathbf{C}}^T_{k+1}(\tilde{\mathbf{C}}_{k+1}\tilde{\mathbf{C}}^T_{k+1} + \mathbf{R}_{\nu_{k+1}})^{-1}$ and $\tilde{\mathbf{C}}_{k+1} = \tilde{\mathbf{H}}\mathbf{S}^-_{x_{k+1}}$, we obtain the evolvement of $\mathbf{S}_{x_{k+1}}$ as:

$$\hat{\mathbf{S}}_{x_{k+1}} = \mathbf{S}^-_{x_{k+1}}\tilde{\mathbf{V}}_{k+1}\sqrt{\tilde{\mathbf{D}}_{k+1}} \tag{11}$$

where $\tilde{\mathbf{V}}_{k+1}\tilde{\mathbf{D}}_{k+1}\tilde{\mathbf{V}}^T_{k+1} = (\mathbf{I} - \tilde{\mathbf{K}}_{k+1}\tilde{\mathbf{C}}_{k+1})$, the computation of which requires eigendecomposition on a $n \times n$ matrix.

The reduced-rank strategy can be easily coupled to this SR structure:

$$\begin{aligned}
\mathbf{G}^q_{k+1} &= \mathbf{S}^{q-}_{x_{k+1}}\tilde{\mathbf{K}}^q_{k+1} \qquad (12)\\
\hat{\mathbf{X}}_{k+1} &= \bar{\mathbf{X}}^-_{k+1} + \mathbf{G}^q_{k+1}(\mathbf{Y}_{k+1} - \tilde{\mathbf{H}}\bar{\mathbf{X}}^-_{k+1})\\
\hat{\mathbf{S}}^q_{x_{k+1}} &= \mathbf{S}^{q-}_{x_{k+1}}\tilde{\mathbf{V}}^q_{k+1}\sqrt{\tilde{\mathbf{D}}^q_{k+1}}
\end{aligned}$$

where $\tilde{\mathbf{K}}^q_{k+1} = \tilde{\mathbf{C}}^{qT}_{k+1}(\tilde{\mathbf{C}}^q_{k+1}\tilde{\mathbf{C}}^{qT}_{k+1} + \mathbf{R}_{\nu_{k+1}})^{-1}$ and $\tilde{\mathbf{C}}^q_{k+1} = \tilde{\mathbf{H}}\mathbf{S}^{q-}_{x_{k+1}}$. $\tilde{\mathbf{V}}^q_{k+1}$ and $\tilde{\mathbf{D}}^q_{k+1}$ can be computed from the efficient eigendecomposition of the $q \times q$ matrix $\mathbf{I} - \tilde{\mathbf{K}}^q_{k+1}\tilde{\mathbf{C}}^q_{k+1}$ instead of the original $n \times n$ matrix, alleviating the computational requirement of the original SR structure.

4. EXPERIMENTS

Phantom experiments regarding normal cardiac conditions and right bundle branch blocks (RBBB) are performed to evaluate the effect of RRSR structure on the accuracy of the TMP estimates and computational time. With geometry and fiber information provided by [8], the ventricular mass is represented by 836 meshfree points with detailed 3D fiber structure. The torso, given geometry in [9], is described by triangulated body surface with 330 vertices selected as electrode positions. The simple 2-variable model from [10] is adopted as the TMP activity model. TMP estimation always utilizes models parametrized with standard values defined in [10], while the models used in generating *true* TMP and BSP are modified according to the pathological condition under study, and the parameters are always deviated from standard values by WGN with means equal to 10% of the standard values. Simulated BSPs are contaminated with 10dB white Gaussian noise (WGN) as inputs for TMP estimation.

(a) TMP reconstruction with full rank filtering

(b) TMP reconstruction with RRSR filtering ($q = 400$)

Fig. 2. Volumetric myocardial TMP dynamics in RBBB cardiac conditions, reconstructed with (a) standard filtering with full rank error covariance, and (b) RRSR filtering with $q = 400 \approx 54\%n$. The blue and red in the color bar encodes the minimum and maximum of TMP values, and black contours represent TMP isochrones.

Fig. 1 (a) lists the change of TMP estimation accuracy with increasing rank size q for TMP imaging in normal cardiac conditions and RBBB. The error of TMP estimates is measured by its relative root mean squared root error (RRMSE) against the ground truth, and divided by the RRMSE value obtained in full-rank filtering. As shown, the degrading of the accuracy of TMP estimates remains below 20% in normal conditions when q is reduced to $100 = 12\%n$. In RBBB, there is a relatively more notable decline of the accuracy where q decreases to 600. It is reasonable because the pathological condition introduce more model errors and requires a larger value of q to track the same percent of dominant components. Fig. 1 (b) lists the corresponding change of computational time, which is also normalized by the time used in full-rank filtering. It is evident that, when q drops, the computational time exhibits much more rapid decreasing than the estimation accuracy, where around 90% reduction is achieved with $q = 12\%n$. Fig. 2 compares the TMP imaging results in RBBB using the full and q-rank filtering at $q = 54\%n$. As illustrated, TMP estimates with computational reduction is close to that without reduction, where transmural conduction abnormality is well reconstructed.

These experiments demonstrate the ability of RRSR filtering to bring substantial reduction of computational time of 3D TMP imaging at minor expense of accuracy degrading. It also shows its potential applicability in different cardiac conditions. Real-data studies will be performed in the future, as well the incorporation of adaptive q into the framework.

5. REFERENCES

[1] S. J. Julier and J. K. Uhlmann, "A new extension of the kalman filter to nonlinear systems," in *Proc. Int. Symp. Aerospace/Defense Sensing, Simul. and Controls*, 1997, pp. 182–193.

[2] L. W. Wang, H. Y. Zhang, H. F. Liu, and P. C. Shi, "Imaging of 3d cardiac electrical activity: A model-based recovery framework," in *MICCAI*, 2006, vol. 1, pp. 792–799.

[3] L. Wang, G. Libert, and P. Minneback, "A singular value decomposition based kalman filter algorithm," in *Proc. Industrial Electronics, Control, Instrumentation and Automation*.

[4] I. Fukumori and P. Malanotte-Rizzoli, "An approximate kalman filter for occean data assimilation: an example with one idealized guilf stream model," *J. Geophys. Res*, vol. 100, pp. 6777–6793, 1995.

[5] P. F. Lermusiaux and A. R. Robinson, "Data assimilation via error subspace statistical estimation. part i: theory and schemes," *Monthly Weather Review*, vol. 127, pp. 1385–1407, 1999.

[6] R. Van der Merwe and E. A. Wan, "The square–root unscented kalman filter for state and parameter-estimation," in *Proc. ICASSP*, 2001, pp. 3461–3464.

[7] L. Wang, H. Zhang, C. L. Wang, and P. Shi, "Coupled meshfree-bem platform for electrocardiographic simulation," Tech. Rep., Golisano College of Computing and Information Science, Rochester Institute of Technology, Rochester, NY, USA, July 2008.

[8] M. Nash, *Mechanics and Material Properties of the Heart using an Anatomically Accurate Mathematical Model*, Ph.D. thesis, Univ. of Auckland, New Zealand, May 1998.

[9] R.S. MacLeod, C.R. Johnson, and P.R. Ershler, "Construction of an inhomogeneous model of the human torso for use in computational electrocardiography," in *IEEE EMBS*, 1991, pp. 688–689.

[10] R. R. Aliev and A. V. Panfilov, "A simple two-variable model of cardiac excitation," *Chaos, Solitions & Fractals*, vol. 7, no. 3, pp. 293–301, 1996.